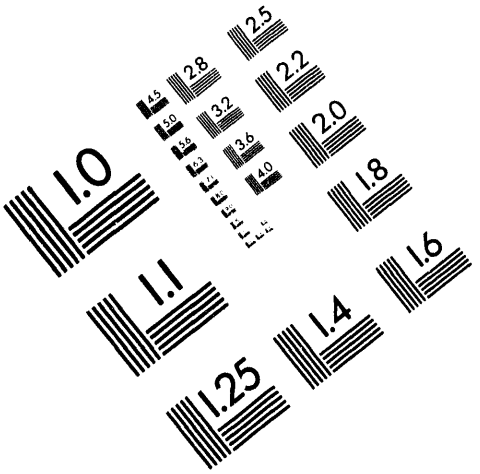

AIIM

Association for Information and Image Management

1100 Wayne Avenue, Suite 1100
Silver Spring, Maryland 20910

301/587-8202

Centimeter

1 2 3 4 5 6 7 8 9 10 11 12 13 14 15 mm

1 2 3 4 5

Inches

MANUFACTURED TO AIIM STANDARDS
BY APPLIED IMAGE, INC.

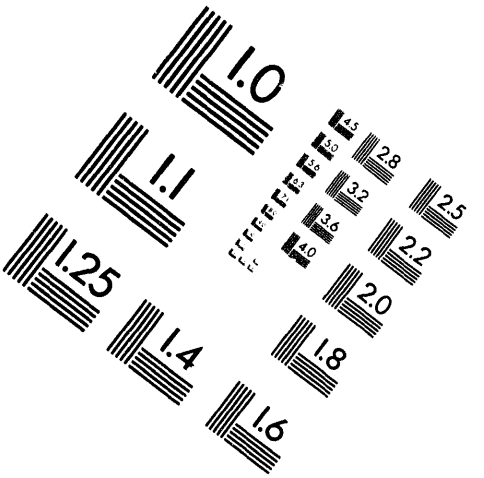

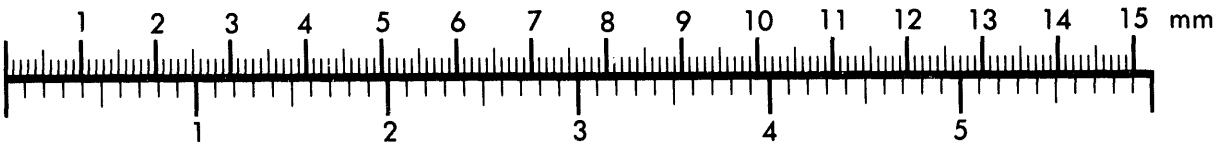

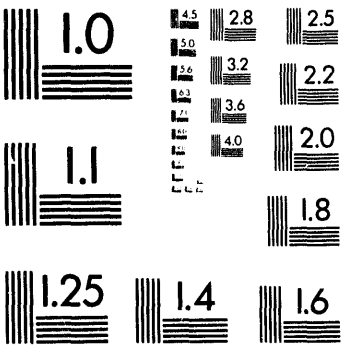

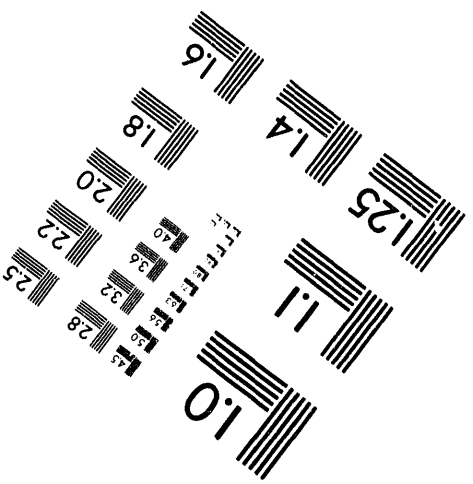

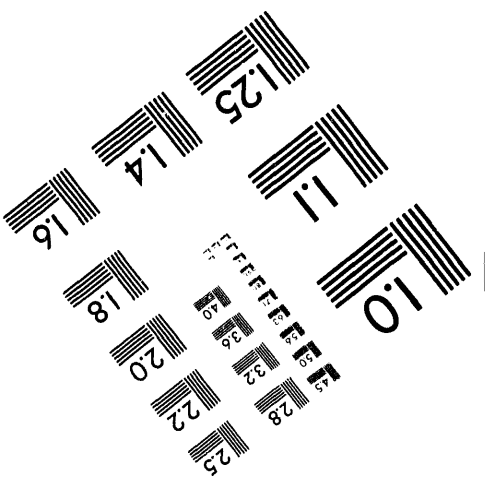

1 of 1

Conf-9406261--1

PNL-SA-24865

HIGH TEMPERATURE CORROSION AND CRACK GROWTH OF SIC/SIC AT VARIABLE OXYGEN PARTIAL PRESSURES

R. H. Jones
C. H. Henager, Jr.
C. F. Windisch, Jr.

June 1994

Presented at the
Japan-USA Seminar Development and Environmental
Characteristics of New Materials
June 7-9, 1994
Mt. Hood, Oregon

Prepared for
the U.S. Department of Energy
under Contract DE-AC06-76RLO 1830

Pacific Northwest Laboratory
Richland, Washington 99352

DISCLAIMER

This report was prepared as an account of work sponsored by an agency of the United States Government. Neither the United States Government nor any agency thereof, nor any of their employees, makes any warranty, express or implied, or assumes any legal liability or responsibility for the accuracy, completeness, or usefulness of any information, apparatus, product, or process disclosed, or represents that its use would not infringe privately owned rights. Reference herein to any specific commercial product, process, or service by trade name, trademark, manufacturer, or otherwise does not necessarily constitute or imply its endorsement, recommendation, or favoring by the United States Government or any agency thereof. The views and opinions of authors expressed herein do not necessarily state or reflect those of the United States Government or any agency thereof.

MASTER

DISTRIBUTION OF THIS DOCUMENT IS UNLIMITED

HIGH-TEMPERATURE CORROSION AND CRACK GROWTH OF SiC/SiC AT VARIABLE OXYGEN PARTIAL PRESSURES

R.H. Jones, C.H. Henager, Jr. and C.F. Windisch, Jr.
Pacific Northwest Laboratory
Richland, Washington 99352

ABSTRACT

Thermal gravimetric analysis (TGA) and subcritical crack growth (SCG) measurements of chemical-vapor-ilfiltrated (CVI)-SiC matrix, reinforced with Nicalon[R] fibers and with a 1-μm-thick C fiber/matrix interface, have been conducted at 1100°C over O_2/Ar mixtures ranging from 0.25% to 20.0% O_2. The TGA and interface recession measurements both gave linear reaction kinetics for O_2 concentrations of 2.0% or less and a reaction order of unity. Subcritical crack-growth measurements demonstrated that crack velocity in the stress intensity-independent Stage II regime increases with increasing O_2/Ar ratio. Also, the transition from Stage II to the stress intensity-dependent Stage III regime is shifted to lower stress intensities with increasing O_2/Ar ratio. A time-dependent crack-growth model that incorporates creep of the bridging SiC fibers and the removal of the C interfacial layer by oxidation successfully explains the subcritical crack-growth characteristics.

Introduction

Continuous fiber-reinforced ceramic matrix composites (CMCs) are being developed for high-temperature applications such as turbine combustors, heat exchangers, fusion reactor first wall and blanket, and boilers. Composite materials with SiC, Si_3N_4 and Al_2O_3 as either the matrix or fiber reinforcement are being developed. These materials have been chosen for their high-temperature strength and corrosion resistance; however, the desired fracture toughness is imparted by a thin interface layer between the matrix and fiber. This interface layer provides load transfer to the fiber combined with an interface fracture strength that provides pseudoductility to these ceramic/ceramic composite materials. This pseudoductility results from the energy absorbed during interface

fracture and fiber pull-out at stresses exceeding the fiber interface fracture strength.

A 200-to 1000-nm-thick fiber/matrix interfacial layer of C or BN has been used successfully in many of these composite materials; however, the stability of these materials in oxidizing environments is a long-term durability concern. Therefore, although SiC and Si_3N_4 form a protective SiO_2 layer in oxidizing environments, loss of the fiber/matrix interfacial layer will seriously degrade these composites' structural properties. This paper reports the effects of oxygen partial pressure on the weight loss and time-dependent SCG of SiC/SiC composites with either C or BN as the fiber/matrix interfacial layer.

Experimental Technique

Material

The CMC material tested was fabricated by Refractory Composites, Inc. of Whittier, CA, and consisted of 4-mm-thick pieces of 8-ply Nicalon fiber cloth (0°/90°) and CVI ß-SiC. The C interfaces were deposited on the Nicalon fibers before the ß-SiC CVI fabrication step. The photomicrograph of the material in Fig. 1 shows a region with the fibers in cross section. The fiber diameter was measured to be 15 ± 2 μm and the C interface was approximately 1.0 ± 0.2 μm thick.

Thermal Gravimetric Analysis

Samples with dimensions of about 4 x 4 x 8 mm were tested at 1100°C using TGA. One face of the sample was cut so that it was free of the SiC coating applied to the surface of the material during the last phase of fabrication. All other faces of the samples had a thin (approximately 5 μm-thick) SiC coating. Post-testing analysis of specimens revealed that only the uncoated surfaces had reacted. Consequently, all rates were normalized with respect to the cut, uncoated surface. Samples tested at 800°C, 900°C and 1000°C were cut to the dimensions of about 4 x 4 x 4 mm. Unlike the larger samples, they had two uncoated surfaces, so all rates for these samples were normalized with respect to the sum of these two surfaces. Comparison of data for the two size samples revealed consistent behavior. Coincidentally, the total area of the uncoated surfaces was also similar for the two geometries, ranging

from a low of about 0.30 cm^2 for the larger specimens to a high of about 0.40 cm^2 for the smaller ones.

TGA studies were performed using a Netzsch STA409 thermogravometric analyzer. Gas flow was maintained at about 1 SCFH through the instrument furnace and composition was controlled using an MKS 147 multi-gas controller with O_2 content displayed on a Thermox meter. Mixtures of O_2 with Ar were used in these experiments. In each test, a sample was placed in an alumina cup in the analyzer furnace. The furnace was then sealed, gas flow was adjusted, and the balance was allowed to equilibrate for about 2 h before heatup. This approach minimized the effect of experimental drift that was most noticeable during the first hour. The temperature was then controlled according to the following program: 1) a ramped heatup to the temperature of interest within 0.5 h, 2) a hold at the temperature of interest for 3 to 12 h, and 3) a cooldown to ambient temperature that took 2 h or more. Throughout the test, mass change was recorded using a Netzsch analog recorder with an accuracy of about 0.1 mg. Traces showed some irreproducibility within the first few minutes after attaining the set temperature. This irreproducibility was attributed to both mass loss and experimental drift during heatup. The latter was determined to be equivalent to about a 1 mg increment by performing the same experiment on dry Al_2O_3 powder. Treatment of the SiC/SiC material in Ar at 1100°C revealed no significant mass change, so all the results were attributed to reactions involving O_2

Subcritical Crack Growth

The SCG studies were performed using constant load tests for times up to 1 x 105 s, giving long-term crack velocity data, and using stepped-load tests with load holding times of 1000 s carried out at 1100°C in Ar and Ar plus varying O_2 levels. Single-edge-notched bend bar (SENB) specimens with dimensions of 4 x 5.5 x 50 mm were tested in 4-point bending using a fully articulated SiC bend fixture.[1-3] The specimens were typically loaded at an applied stress intensity of 7 to 8 MPa$\sqrt{m}$ to begin the test. The test continued until a load drop was observed. Specimens that were tested in Ar plus O_2 were brought up to temperature in pure Ar.

The displacement-time curves for the 1000-s exposures at constant load in Ar indicate that the specimen displacement, and thus the crack-

opening displacement, undergoes a transient period of displacement that is logarithmic in time over the 1000-s hold time. The slope of the displacement-time curve over the final 600 s of the load step was taken as proportional to the crack velocity for each 1000-s period. The longer-term hold displacement-time data were fit to polynomial functions and differentiated to give $\partial\delta/\partial t$.

Writing $\delta = P\,C(a)$, where δ is the displacement, P is the load, C is the specimen mid-point compliance, and a is equal to a/W (normalized crack length) gives

$$\frac{\partial\delta}{\partial t} = \frac{\partial}{\partial t}(P\,C(\alpha)) = P\,\frac{\partial C}{\partial \alpha}\frac{\partial \alpha}{\partial t} = \frac{P}{W}\frac{\partial C}{\partial \alpha}\frac{da}{dt} \qquad (1)$$

which is used to derive an expression for da/dt (V_c):

$$\frac{da}{dt} = V_c = \frac{\frac{\partial\delta}{\partial t}W}{P\,C'(\alpha)} \qquad (2)$$

where V_c is the crack velocity and W is the specimen thickness. An expression was determined for the mid-point compliance of a SENB specimen in 4-point bending and was used to calculate crack length and $C'(a)$.[2] The slope of the displacement-time curve at a given load is $\partial\delta/\partial t$.

The instantaneous specimen compliance at any point along the corrected load-deflection curve was calculated as the slope of the line from the origin to any point on the load-deflection curve. Bridging-zone contributions to the specimen compliance were not included (i.e., the cracks, for the purposes of the compliance calculations, were idealized as unbridged elastic cracks obeying linear-elastic fracture mechanics). It is recognized that this assumption is not true and causes errors in crack-length calculations (see Discussion).[4] However, visual observations of crack length during the test were not possible, and without detailed knowledge of the bridging zone the specimen compliance cannot be corrected for bridging fiber contributions. Therefore, all references to crack length, velocity, and stress intensity are made with the understanding that the reference is to an effective elastic crack.[4] Data are presented in the discussion comparing calculated and measured crack lengths (from sacrificial specimens) that reveal the crack lengths are overpredicted by about 35%.

Experimental Results

Thermal Gravimetric Analysis

TGA mass losses as a function of time for CMC materials at 1100°C are shown in Fig. 2 for four O_2 partial pressures. The data are nearly linear at 0.5%, 1.0%, and 2.0% O_2 within the first 3 to 6 h. At 20% O_2 (approximately air), the data are nonlinear, showing a very rapid mass loss within the first 2 h and then apparently "saturating" with no additional significant mass change. As shown in Fig. 3, the mass losses varied parabolically with time when the O_2 was 0.25% (compare to 0.5%), especially at longer times. For the purpose of this analysis, however, the variation at 0.25% and 1100°C under 3 h was considered nearly linear.

After the TGA tests, samples were cut and polished for microscopic examination. Similar to previous studies by Henager and Jones,[3] the samples showed evidence of C-interface removal as a result of exposure to O_2-containing environments. In the present study, this interface removal proceeded along a surprisingly uniform reaction front at a rate that depended on the O_2 partial pressure. Fig. 1 shows a photomicrograph of the cross section of one of the CMC samples after exposure to 0.5% O_2 for 6 h at 1100°C. A clearly defined reaction front can be seen between 600 and 900 μm, which define the high and low positions, from the exposed surface in this sample. Between this front and the surface, almost all of the C interface was removed; below this front, the C interface appears largely intact.

The morphology of the C interface at the reaction front varies somewhat within two samples shown in Fig. 4. In the left sample, the C-interface appears uniformly attacked across the interface width; in the right sample, the reaction is slower at the fiber/carbon and carbon/matrix interfaces. In the latter case, a channel appears to form near the center of the interface material, suggesting that C attached to the matrix and fiber may be less reactive.

Similar C-interface recession morphologies were observed for samples treated at other O_2 partial pressures at 1100°C, although the depth of recession for samples treated for the same time increased with increasing O_2 partial pressure. Average recession rates were determined by dividing the average recession depth (average of high and low positions of the reaction front) by the time of exposure for samples tested at 0.25%, 0.5%, 1.0%, and 2.0% O_2 and these are plotted against the O_2 partial pressure in a log-log format in Fig. 5. The error bars for these data

reflect both the uncertainties in the position of the reaction front in a given sample determined from the difference between the high versus low positions (giving $\pm 7 \times 10^{-7}$ cm/s) and the variations of results for different samples tested under the same conditions ($\pm 1.2 \times 10^{-6}$ cm/s).

As shown in Fig. 5, the relationship between the measured recession rates and O_2 partial pressure is nearly linear. The slope calculated by linear regression indicates a reaction order with respect to O_2 of 0.9 ±0.2 or about unity. The intercept of the regression gives the rate at 1 atm O_2, $k_{1\ atm}$, equal to 4 (±2) x 10^{-4} cm/s at 1100° C.

The TGA mass loss data were also used to determine the recession rates for the various O_2 partial pressures. A number of assumptions were used in this analysis. Most importantly, it was assumed that all of the mass loss was associated with C-interface removal. This assumption may not be completely accurate since other sources of oxidizable C are present, including the SiC matrix, the Nicalon fibers, and the exposed sample surface. There is up to 14% excess C in SiC fibers and even more within 200 nm of the surface, including a 30-nm surface region containing mainly C.[5]

The recession rates (RR) were calculated from the TGA data for experiments at 0.25%, 0.5%, 1.0%, and 2.0% O_2 at 1100°C using the following relationship:

$$RR = ML/t \times 1/r \times 1/A_I \qquad (3)$$

where ML is the mass loss at time t, and ML/t is the rate of mass loss or the slope of the time vs mass loss curves in g/s (Fig. 2). Duplicate experiments gave slopes that agreed to within 5% of each other. The density of the C interface, r, is taken as 2 g/cm^3; and A_I, the total area of the C interface for the whole exposed surface, was determined by image analysis of the surface and found to be 8.6 (±0.5) x 10^{-3} cm^2.

The recession rates calculated from the mass loss rates using Equation 3 are plotted in Fig. 5 for comparison with the geometrically measured values. Again, the data are quite linear with a slope of 0.8 ±0.1, which agrees with the value for the reaction order obtained from the TGA mass-loss data.

Subcritical Crack Growth

The data for the C-interface materials, when plotted as crack velocity versus applied stress intensity (V-K curves), reveal a stage-II region

where the crack velocity is essentially independent of the applied stress intensity Fig. 6 followed by a Stage III, or power-law crack-growth region, at high stress intensities.

The power-law region exhibits a strong dependence, but the Stage II region exhibits a weak dependence, on the applied stress intensity. The data reveal a measurable increase in Stage II crack velocity because of O_2 in the gas. The crack velocity increases with increasing O_2 content for the C-interface material (Figs. 6 and 7). Also, the stress intensity required for the onset of stage III is shifted to a lower value of the applied stress intensity.

Model of Oxygen Effects on Crack Growth

A discrete, 2-dimensional micromechanics model was developed to understand the effects of the fiber-bridging zone on crack-tip stress intensities and to predict crack velocities for an idealized composite under conditions of fiber creep and interface removal. Although other models[6-12] have been developed to describe crack-wake bridging in continuous-fiber composites (CFC), it is desirable to have a discrete model that allows numerical calculations of crack-closure forces and is amenable to time-dependent calculations. The model developed here places a semi-infinite crack in a linear-elastic body and simulates the bridging fibers by crack closure forces placed along the crack face. The forces applied by the fibers to the crack face are calculated using an explicit frictional bridging model[9] that describes the fiber load transfer as a function of distance from the crack tip. The modeling performed here is similar in many respects to that performed by Davidson[13] and has been presented by the authors elsewhere.[2]

The details of the bridging-zone calculation require knowledge of the interfacial shear strength and fiber fracture strength. The value of the interface strength determines the stress on a given fiber in the bridging zone. The fiber fracture strength then determines the length of the bridging zone based on the last unfailed fiber, and together these determine the amount of crack-tip screening for an equilibrium bridging zone. An independent estimate of the interfacial shear strength gives a nominal value for the interface strength equal to or less than about 35 MPa. It would be expected that this shear strength would be less than 35 MPa at 1100°C because of the thermal expansion mismatch of the Nicalon fibers and the β-SiC matrix. Data[14] for strengths of Nicalon fibers at elevated temperatures in air indicate that 1.5 GPa at 1100°C is

an average strength value. Therefore, values for the interfacial shear strength, τ, ranging from 10 MPa to 50 MPa and a fiber fracture strength, σ_f^c, equal to or less than 1.5 GPa are chosen for the calculations performed later. Additionally, E_m = 400 GPa and E_f = 200 GPa are chosen as representative elastic moduli for matrix and fiber, respectively. A nominal fiber radius of 5 μm is used for r_f. The fiber failure stress (σ_f^c) is used to define the bridging-zone length for frictional bridging. The length of the bridging zone is defined as e distance from the crack tip to the last unfailed fiber.

A comprehensive model of subcritical crack growth in CFC materials must take into account all possible time-dependent behaviors in the crack-wake bridging zone. These include fiber creep, fiber/matrix interface creep, possible visco-elastic effects at the interface, and time-dependent interface removal due to oxidation. The net effect of any time-dependent deformation in the crack-wake region is to relax the crack-closure forces. Fiber creep undoubtedly plays a role since the bridging fibers are highly stressed in the crack-wake region and are being held at those loads for long times. Interface removal must also be important based on the TGA and optical microscopy results. It is unlikely that viscous or glassy phases are being formed because the SCG experiments are performed in argon or argon with small amounts of oxygen.

Available creep data for Nicalon fibers at 1100°C in pure Ar[15] were used to construct a constitutive equation for the stress and time dependence of creep in Nicalon fibers at 1100°C. A stress relaxation calculation for Nicalon fibers undergoing creep was performed by partitioning the total fiber strain into elastic and plastic (creep) components and by requiring that the total strain rate be zero such that the fiber elastic strain is replaced by plastic strain.

The mechanics of frictional bridging is typically given in terms of a interface-debond length (λ), interfacial shear strength (τ), crack-opening displacement (u), and fiber stress (σ_f) (Fig. 8). The fiber/matrix debond crack length is determined by the interfacial shear strength and crack-opening displacement. The effect of oxygen and subsequent interface removal on the bridging mechanics is simulated by allowing this debond crack length, λ, to become time-dependent. As λ increases due to interface removal, the fiber is gradually decoupled from the matrix; therefore, σ_f must decrease with time due to interface removal. In terms of existing mechanics models, the debond crack length can be related to the interfacial shear strength as

$$\lambda^2 = \frac{u\, r_f\, E_f}{\tau\,(1+\eta)}\ ,\ \eta = \frac{E_f\, V_f}{E_m\, V_m} \qquad (4)$$

and the fiber stress is then related to λ through the following relation to the interfacial shear strength, τ, as;

$$\sigma_f = 2\left(\frac{u\, E_f\, \tau(1+\eta)}{r_f}\right)^{\frac{1}{2}} \qquad (5)$$

The TGA and optical microscopy data can be used to calculate the time dependence of λ and, therefore, τ and σ_f. Model results for fiber stress as a function of time in the crack wake due to fiber creep only, and additionally, due to interface removal are shown in Fig. 9. It can be seen that the model predicts faster relaxation due to fiber creep plus interface removal compared to fiber creep only.

Given these time-dependent quantities, the discrete micromechanics model can be used to calculate the crack velocity using a quasi-static approach given these time-dependent quantities. A quasi-static approximation to the crack velocity assumes that the bridging zone is in equilibrium by virtue of a balance between crack advance and relaxation of bridging-zone stresses. As the crack advances, it bridges additional fibers, which retards its growth. As the stresses in the bridging zone relax, the crack-tip screening is reduced and the crack tends to advance. This assumption does not require detailed information about the physical mechanism of crack advance due to matrix cracking.

The quasi-static approximation assumes that the stress intensity at the crack tip is a constant such that

$$K_{tip}(a,t) = C \Rightarrow dK_{tip} = 0 \qquad (6)$$

Therefore, one can write the total differential of K_{tip} as

$$dK_{tip} = \frac{\partial K_{tip}}{\partial a}\, da + \frac{\partial K_{tip}}{\partial t}\, dt \qquad (7)$$

which can be used to derive an expression for crack velocity, V_c, as

$$V_c = \frac{da}{dt} = -\left(\frac{\frac{\partial K_{tip}}{\partial t}}{\frac{\partial K_{tip}}{\partial a}}\right) \qquad (8)$$

where the crack velocity is expressed as the ratio between the time dependence of K_{tip} due to stress relaxation of bridging forces, $\partial K_{tip}/\partial t$, and the change in K_{tip} due to crack advance, $\partial K_{tip}/\partial a$.

Values for $\partial K_{tip}/\partial t$ can be calculated from differentiating a polynomial fit to K_{tip} data calculated as a function of time due to fiber creep and interface removal, Fig. 10 for varying pO_2. For this case, the fiber volume fraction (V_f) was set to 0.3, τ was set to 10 MPa, and K_A was set to 10 MPa$\sqrt{m}$. The bridging zone was 300 μm long and contained 19 intact bridging fibers. The rate of change of K_{tip} with respect to a is readily calculated from the bridging model by computing K_{tip} for incremental changes in crack length. For a given choice of model parameters, or material constants, this quantity is a constant.

The quasi-static approximation gives a range of crack velocities depending on the rate of stress relaxation of the fiber bridging stresses, given that $\partial Ktip/\partial a$ is a constant (Fig. 11). The model results clearly show that the additional stress relaxation in the bridging fibers caused by interface removal acts to increase the crack velocity compared to pure Ar, where fiber creep only is occurring.

Discussion

The data presented here are given in terms of the length and velocity of an effective elastic crack, with the applied stress intensity representing the K-field of such a crack. Although this has been adopted by others,[4] it is recognized that the actual crack lengths and velocities will differ from this idealized situation. The presence of large-scale bridging zones in these materials suggests that the use of indirect crack length measurements, such as specimen compliance measurements, will not accurately determine the actual crack length. However, these materials and testing conditions do not allow direct crack-length measurements.

As a first step in determining actual crack lengths for these CFC materials, several specimens were cracked under identical SCG conditions (1100°C in pure Ar), sectioned, and polished to reveal crack lengths and morphologies. A comparison was made between measured and calculated

crack lengths. The experimentally measured instantaneous compliance was used to calculate effective crack lengths using the procedure discussed in the procedure section and this calculated crack length was compared to the crack length measured optically from sectioned and polished specimens. The optical photomicrography revealed that the specimens were multiply cracked, with up to nine separate and equally spaced cracks, at the notch root. The width of this cracked, or damaged, region was approximately equal to 1 mm, or about twice the notch width. Each subcritical crack was fully bridged from the notch root to the crack tip and all the bridging fibers appeared to be intact. The measured crack length was determined from the length of the longest visible crack. The calculated crack lengths are, on average, within 36% of the measured crack lengths. More importantly, the slopes of the two C(a/W) curves are nearly equal, resulting in equal values of dC/da used to compute crack velocities. Therefore, calculated effective crack velocities should accurately reflect the velocity of cracks in the damage zone. Since large-scale bridging of a single crack in an SENB specimen should result in underpredicting the crack length, contrary to what is observed here, the effect of the multiple cracking must be to increase the specimen compliance enough to overpredict actual crack lengths.

Comparison of typical SCG V-K data for monolithic ceramics with the data presented here reveals this distinguishing feature; namely, the appearance of a K-independent regime (stage-II) in the V-K diagram for the CFC material. The power-law dependence of crack velocity observed in monolithic ceramics is replaced by a K-independent, or weakly K-dependent, regime (Stage II) that corresponds to the material's R-curve. This behavior's interpretation is that the extent of the Stage II regime for CFCs corresponds to the formation of the equilibrium bridging zone as the crack extends. Stage II behavior is observed under certain conditions in monolithic materials and in glasses[16-19] when the transport of a critical species to the crack tip is rate controlling. This is analogous to the situation here as the stress relaxation of the crack-wake region is rate controlling. A major distinction is the very weak K-dependence observed here. The exponent of K in Stage II is less than one for the CFC materials, but is typically larger than one for monolithic ceramics.[18-19]

The transition to Stage III, or power-law growth, corresponds to saturation of the bridging zone and the inability of the material to further shield the crack tip from the far-field K_A . It would be reasonable to expect that the crack velocities would revert to a power-law growth rate in Stage III. Indeed, this appears to be the case in Fig. 6; however, only a

limited range of data are available for determining the power-law exponent in the Stage III regime because the specimen fails soon after making the transition. Nevertheless, power-law exponents in the range of 8 to 20 are obtained for the limited data in this study. Exponents in this range are typical of SCG exponents measured for glasses and monolithic ceramics at elevated temperatures[16, 20-28] This behavior is interpreted as power-law crack growth dominated by matrix cracking in the regime where the bridging zone is unable to effectively shield the crack tip from K_A. Therefore, the model described here is not valid for this regime since the quasi-static approximation is not expected to hold. It is worth noting that no models are available to accurately describe SCG of ceramic materials in the power-law regime, although attempts have been made.[19]

The agreement between the model based on fiber creep, and the experimental results is encouraging, Fig. 11. Not only is the absolute magnitude of the crack velocity predicted, but the observed time-dependence of Vc is also rationalized. There are no adjustable parameters in the model and typical values for material constants were assumed.

The model developed here predicts similar results to those obtained by Thouless[7], Nair et al.[6], and Jakus et al.[29] Crack advance is controlled by the time-dependent behavior of the crack-bridging ligaments, whether the relaxation is due to visco-elasticity or thermal creep. The crack-opening displacement and, therefore, the crack-tip stress intensity are shown to obey similar time-dependent relationships.

High-temperature SCG of CFCs is expected to be influenced by the following environment-induced effects, excluding thermal effects, where crack bridging controls the local stress intensity: 1) fiber stability and strength, 2) fiber matrix interface stability, and 3) effects on the viscosity of the grain boundary phase at the crack tip. Therefore, a study on the corrosion and crack-growth behavior of CFCs should evaluate the contribution of these processes to time-dependent composite properties. While a more comprehensive study is in preparation, several important points can be made from these data. The experiment was designed (1100°C and low pO_2) to have negligible effects on fiber stability and strength (30), and to have little or no effects due to oxidation of the SiC matrix material.[31] However, the experimental conditions were such that the C-interfaces would be attacked by the O_2 atmosphere used in this study. Indeed, the only discernible effect of the O_2 was to partially remove these reactive interfaces during the high-temperature exposure.

The addition of O_2 to the 1100°C Ar environment increases the crack velocity in the Stage II regime and shifts the Stage-II-to-Stage-III transition to lower K-values (Fig. 6). The shift to lower K-values for the transition to Stage III crack growth is consistent with a reduction in the closure forces imparted on the crack faces by the bridging fibers. Optical and scanning electron microscopy (SEM) micrographs of the specimens exposed to the O_2 with Ar reveal partial removal of the C interfaces due to oxidation. The TGA data substantiate that this material is removed by relating the specimen mass loss to the interface removal. The removal of this interface material reduces the ability of the matrix to transfer load to the fibers and, in turn, reduces the bridging-zone effectiveness. Since both the oxygen exposure the interface removal began when the SCG test was initiated and are cumulative, the interface removal of the crack bridging fibers should progress, from small at the beginning of the test (small K_A) to larger at the end of the test (large K_A). The principal effects of this gradual interface removal appear to be an increase in crack velocity compared to pure Ar and a shift in the Stage-II-to-Stage-III transition to lower applied stress intensities.

Therefore, in addition to fiber creep causing relaxation of bridging-zone stresses, there will be a time-dependent decrease in the fiber-matrix mechanical coupling as the interface is removed. In turn, this acts to decrease the fiber bridging stress, in accord with Equation 5, and will increase $\partial K_{tip}/\partial t$, as was shown by the model in Fig. 10. Since significant oxidation of interfaces ahead of the crack is neither expected nor observed, $\partial K_{tip}/\partial a$ is expected to remain constant. The net result is an increase in crack velocity, and since the bridging zone as a whole is less effective in screening the crack tip from the applied stress intensity, a shift in the Stage-II-to-Stage-III transition is also expected.

These calculations reveal that relaxation of bridging-zone stresses by any of the above mechanisms, will delay fiber fracture and result in increased available strain energy for crack-tip screening. Therefore, CFCs can actually become tougher and absorb more strain energy in SCG compared to fast fracture. In other words, the amount of crack-wake bridging depends on the temperature, the loading rate, and the constitutive laws obeyed by the bridging ligaments. This is similar to the results found by Steinbrech and Fett for monolithic ceramics [32-34] and the conclusion was the toughness of materials exhibiting R-curve behavior was dependent on specimen history.[33] However, although increases in bridging-zone stress relaxation rates can increase apparent toughness, these same increases will increase $K_{tip}/\partial t$ and SCG velocities, and

mechanical instabilities will be achieved at lower stress intensity values. Experimentally, the Stage-II-to-Stage-III transitions occur at K_A values that are much larger than K_Q, (Fig. 6), and processes that are known to increase bridging-zone stress relaxation rates, such as oxidation-induced interface removal, result in increased SCG velocities and lower Stage-II-to-Stage-III transitions.

Summary

TGA of CMC material consisting of CVI-SiC matrix reinforced with Nicalon fibers and C with 1-μm-thick C interfaces revealed linear kinetics for mass loss within the first 3 to 6 h at a temperature of 1100°C and in 0.25%, 0.5%, 1.0%, and 2.0% O_2. Mass loss at 20% O_2 was rapid and nonlinear. The TGA results, when converted to recession rates involving the C interfaces, compared very well with the recession rates measured geometrically on tested samples that were cross-sectioned for microscopic analysis. The oxidation of the C interface appeared to follow first-order kinetics and the order of the reaction with respect to oxygen appeared to be close to unity.

The velocity of subcritical cracks in CMCs with continuous fibers has been related to the rate of relaxation of fiber-bridging forces in the crack-wake bridging zone. It is proposed that the crack velocity is controlled by the rate of relaxation of the bridging zone stresses by Nicalon fiber creep and a time-dependent change in the fiber-matrix mechanical coupling. A two-dimensional, discrete micromechanics model using a simple constitutive law for creep of Nicalon fibers at 1100°C was able to rationalize measured SCG rates and the time dependence of Vc in continuous-fiber-reinforced b-SiC materials tested in O_2-containing environments. Extension of p(u) functions to the modeling of SCG indicate that knowledge of p(u,t) is required to compute $K_{tip}(t)$ and that such computations are useful in understanding SCG processes for materials with bridged cracks.

Acknowledgments

The assistance of J. L. Humason in performing the TGA and subcritical crack growth measurements is gratefully acknowledged. This research was supported by the U.S. Department of Energy (DOE), Office of Basic Energy Sciences under contract DE-AC06-76RLO 1830 with Pacific Northwest Laboratory, which is operated for DOE by Battelle Memorial Institute.

References

1. C. H. Henager, Jr. and R. H. Jones, *Ceramic Engr. Sci. Proc.,13:7-8* (1992) 411-419.

2. C. H. Henager, Jr. and R. H. Jones, *Mater. Sci. and Engr., A166* (1993) 211-220.

3. C. H. Henager, Jr. and R. H. Jones, *Ceramic Engr. Sci. Proc., 14 [7-8]* (1993) 408-415.

4. A. Bornhauser, K. Kromp, and R. F. Pabst, *J. Mater. Sci., 20* (1985) 2586-2596.

5. Y. Xu and A. Zangvil, *J. Am. Ceram. Soc., 76* (1993) 3034.

6. S. V. Nair, K. Jakus, and T. J. Lardner, *Mech. Mater., 12 [3-4]* (1991) 229-244.

7. M. D. Thouless, *J. Am. Ceram. Soc.,* 71 [6] (1988) 408-413.

8. S. V. Nair and T. -J. Gwo, *J. Engr. Mater. Technol.,* 115 (1993) 273-280.

9. A. G. Evans and R. M. McMeeking, *Acta Metall.,* 34 (1986) 2435-2441.

10. D. B. Marshall, B. N. Cox, and A. G. Evans, *Acta Metall.,* 33 (1985) 2013-2021.

11. B. Budiansky, J. M. Hutchinson, and A. G. Evans, *J. Mech. Phys. Solids*, 34 (1986) 167-189.

12. B. N. Cox and C. S. Lo, *J. Am. Ceram. Soc.,* 40 (1992)1487-1496.

13. D. L. Davidson, *Met. Trans. A,* 23 (1992) 865-879.

14. D. J. Pysher, K. C. Goretta, R. S. Hodder, Jr., and R. E. Tressler, *J. Am. Ceram. Soc.,* 72 (1989) 284-288.

15. G. Simon and A. R. Bunsell, *J. Mater. Sci.,* 19 (1984) 3658-3670.

16. S. M. Weiderhorn, S. W. Freiman, E. R. Fuller, and C. J. Simmons, *J. Mater. Sci.,* 17 (1982) 3460-3478.

17. B. J. Pletka and S. M. Wiederhorn, "Subcritical Crack Growth in Glass-Ceramics," *Fracture Mechanics of Ceramics,* Vol. 4, R. C. Bradt et al., (eds.), Plenum Press, NY, 1978, pp. 745-759.

18. K. D. McHenry and R. E. Tressler, *J. Mater. Sci.,* 12 (1977)1272-1278.

19. H. Cao, B. J. Dalgleish, C. Hsueh, and A. G. Evans, *J. Am. Ceram. Soc.,* 70 [4] (1987) 257-264.

20. S. M. Wiederhorn and L. H. Bolz, *J. Am. Ceram. Soc.,* 53 [10] (1970) 543-548.

21. A. G. Evans, *J. Mater. Sci.,* 7 (1972)1137-1146.

22. A. G. Evans, L. R. Russell, and D. W. Richerson, *Metall. Trans. A,* 6A (1975) 707-716.

23. A. G. Evans and F. F. Lange, *J. Mater. Sci.,* 10 (1975)1659-1664.

24. K. D. McHenry and R. E. Tressler, *J. Mater. Sci.,* 12 (1977) 1272-1278.

25. J. L. Henshall, D. J. Rowcliffe, and J. W. Edington, *J. Am. Ceram. Soc.,* 62 [1-2] (1979) 36-41.

26. J. L. Henshall, *Res Mech.,* 1 (1980) 229-248.

27. J. L. Henshall, "The Mechanism and Mechanics of Subcritical Crack Propagation in Hot-Pressed SiC Above 1000C," *Advances in Fracture Research (Fracture 81),* D. Francois, ed., Pergamon Press, NY, 1981, pp. 1541-1549.

28. P. F. Becher and M. K. Ferber, *Acta Metall.,* 33 [7] (1985) 1217-1221.

29. K. Jakus, J. E. Ritter, and R. H. Schwillinski, *J. Am. Ceram. Soc.*, 76 [1] (1993) 33-38.

30. T. Mah, N. L. Hecht, D. E. McCullum, J. R. Hoenigman, H. M. Kim, A. P. Katz, and H. A. Lipsitt, *J. Mater. Sci.,* 19 (1984)1191-1201.

31. E. A. Gulbransen and S. A. Jansson, *Oxid. Met.,* 4 (1972) 181-201.

32. R. Knehans and R. Steinbrech, *J. Mater. Sci. Lett,* 1 (1982) 327-329.

33. R. Steinbrech, R. Knehans, and W. Schaarwächter, *J. Mater. Sci.,* 18 (1983) 265-270.

34. T. Fett and D. Munz, *J. Am. Ceram. Soc.,* 75 [11] (1992) 3133-3136.

Cross-Section of C-Interface CMC Showing Depth of Interface Removal

1100°C; 0.5% Oxygen; 6 Hours

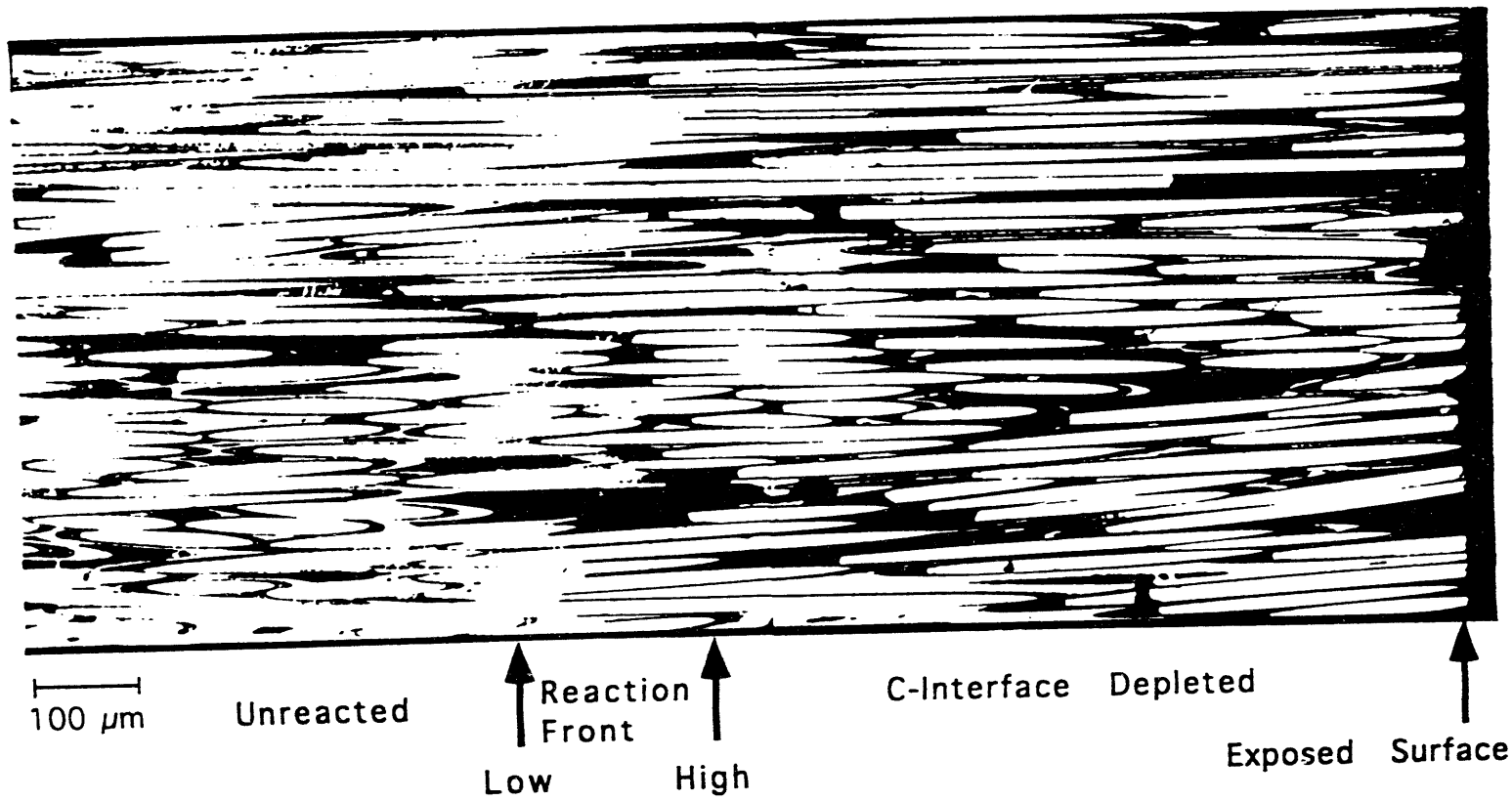

1

SiC/SiC Composites with Carbon Interfaces
TGA Mass Losses at 1100°C

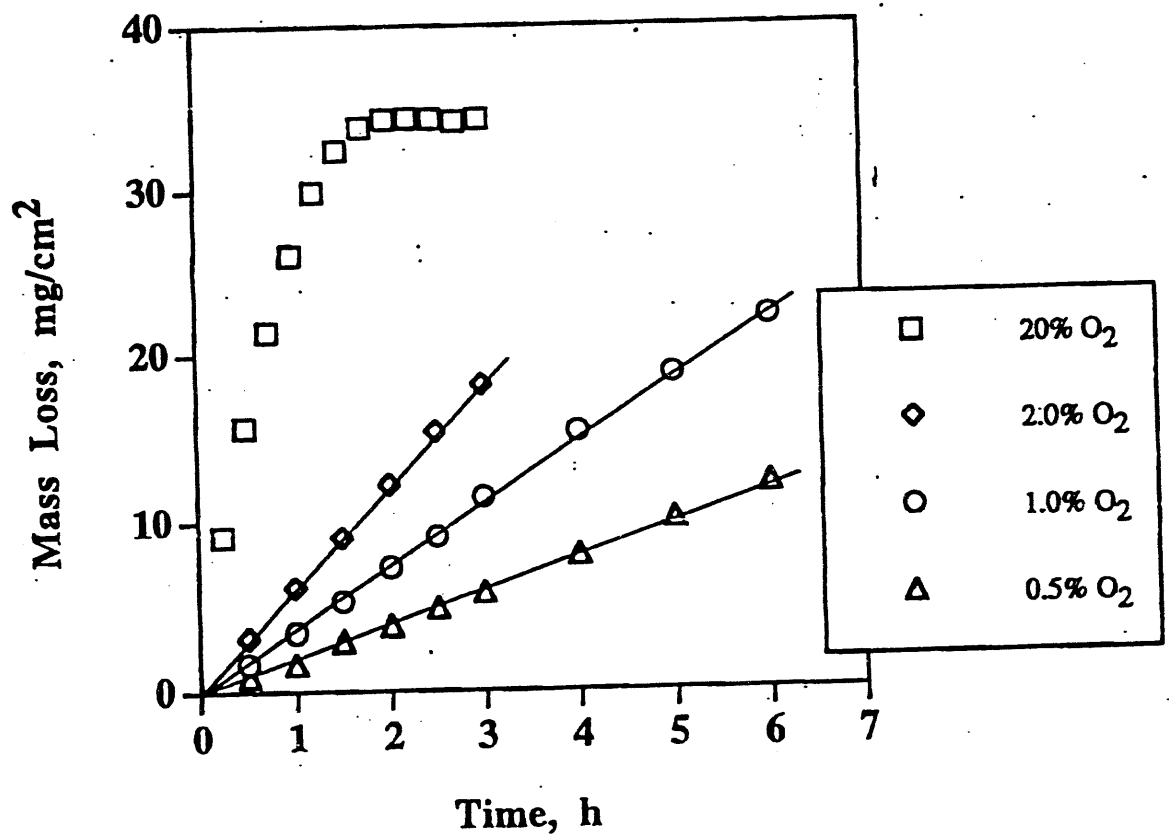

Fig. 2

SiC/SiC Composites with Carbon Interfaces
Nonlinear Behavior at Low pO_2

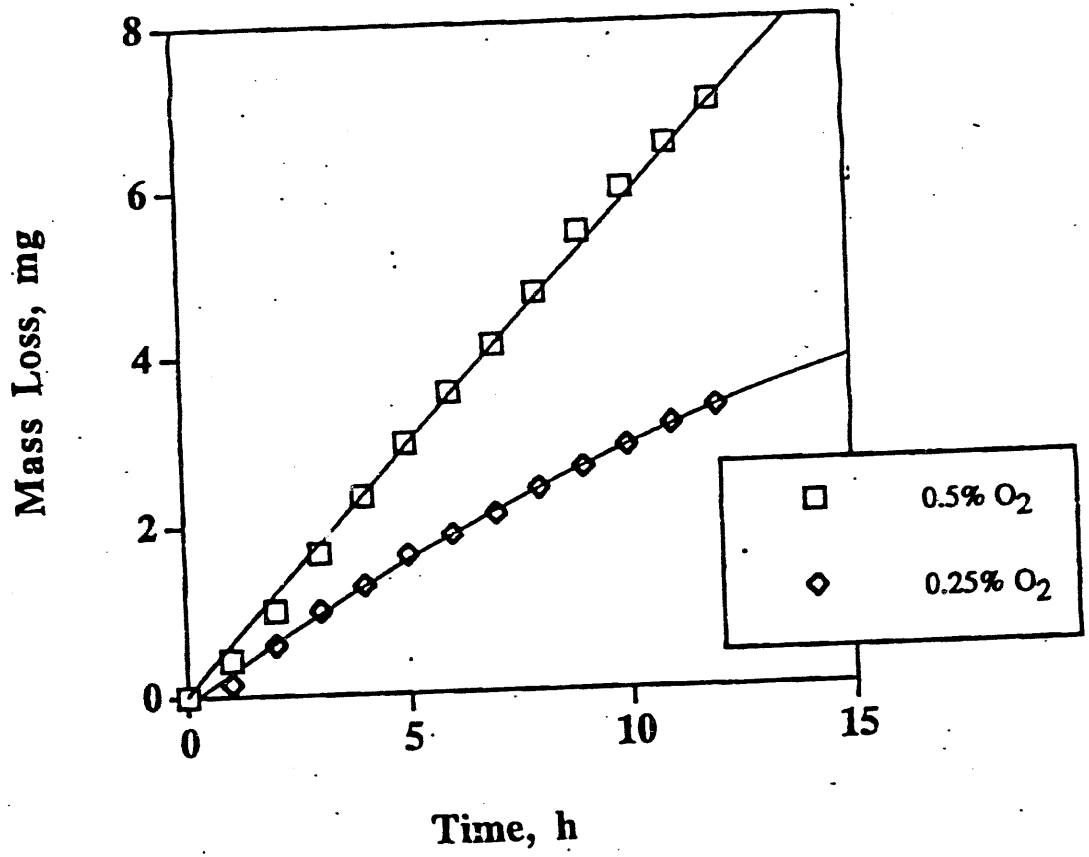

Figure 3

SEM Photomicrographs Showing Different Morphologies at Reaction Front

1100°C; 0.5% Oxygen; 6 Hours

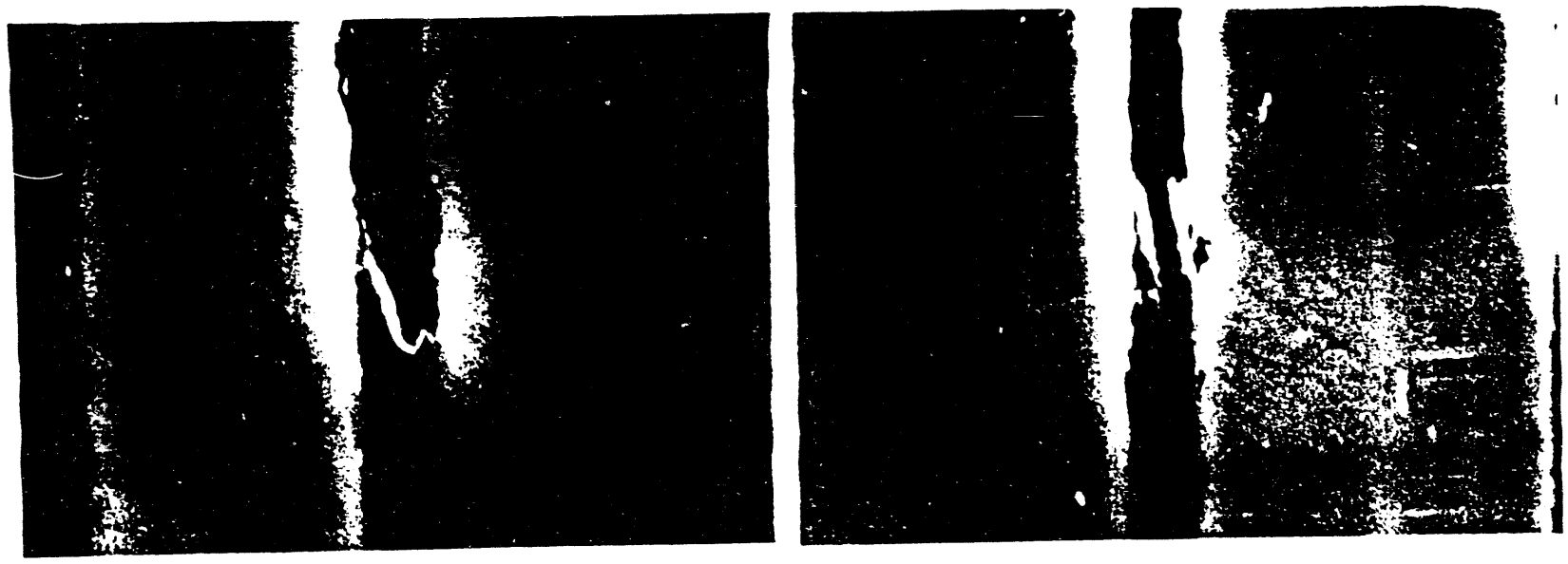

1 μm "Uniform Attack" "Channel Attack"

4

SiC/SiC Composites with Carbon Interfaces
Recession Rates at 1100°C

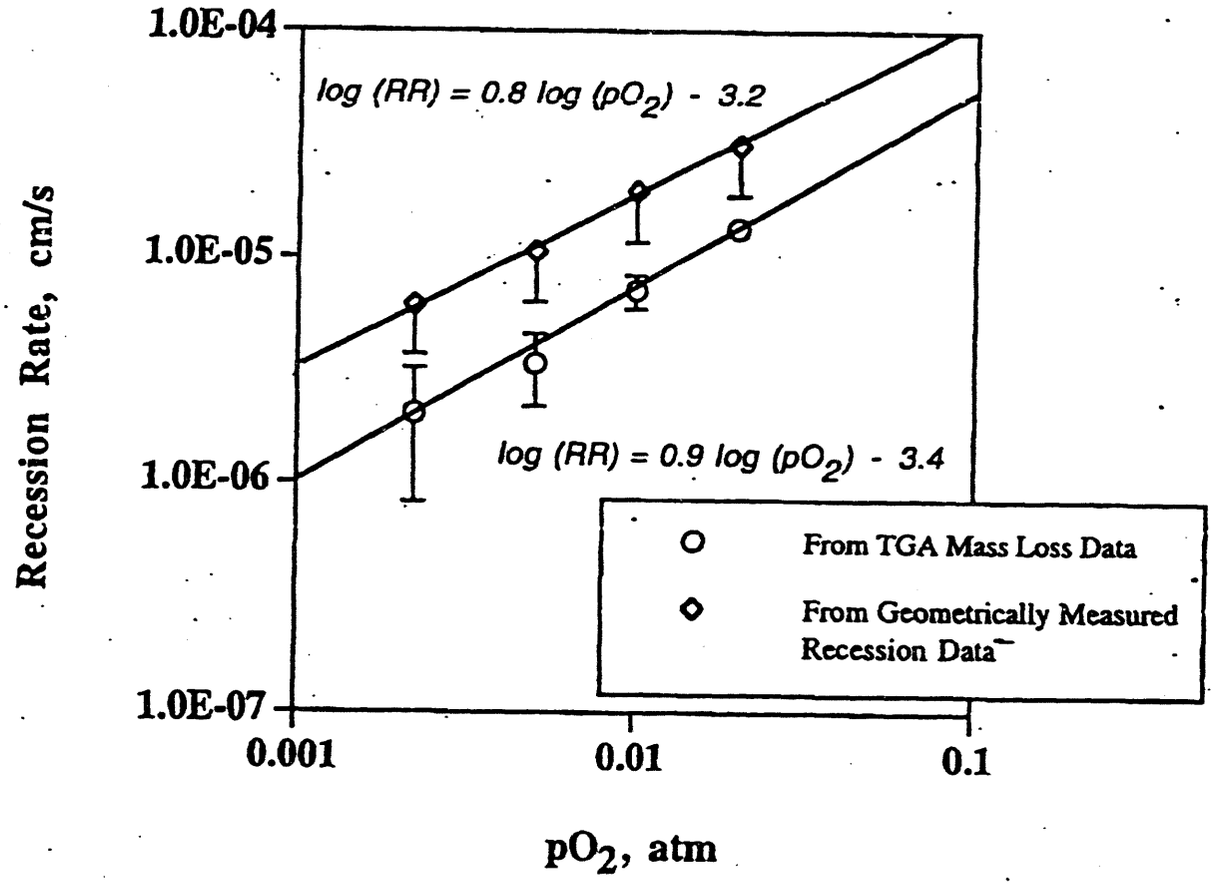

Fig. 5

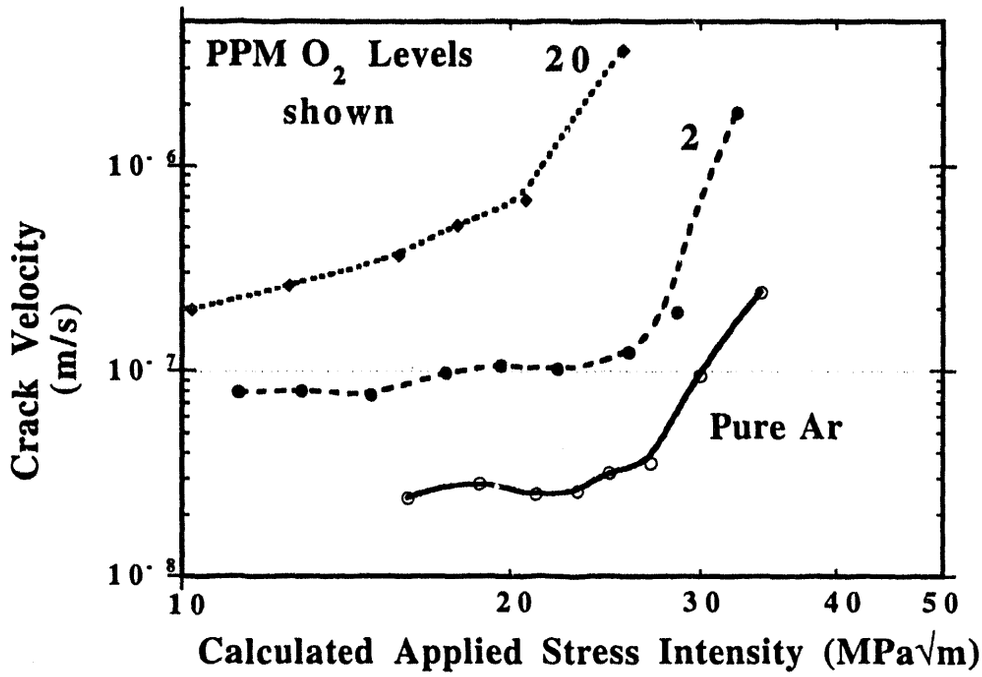

Figure 6. Crack velocity as a function of effective applied stress intensity for pure Ar and two oxygen levels for C-interface material.

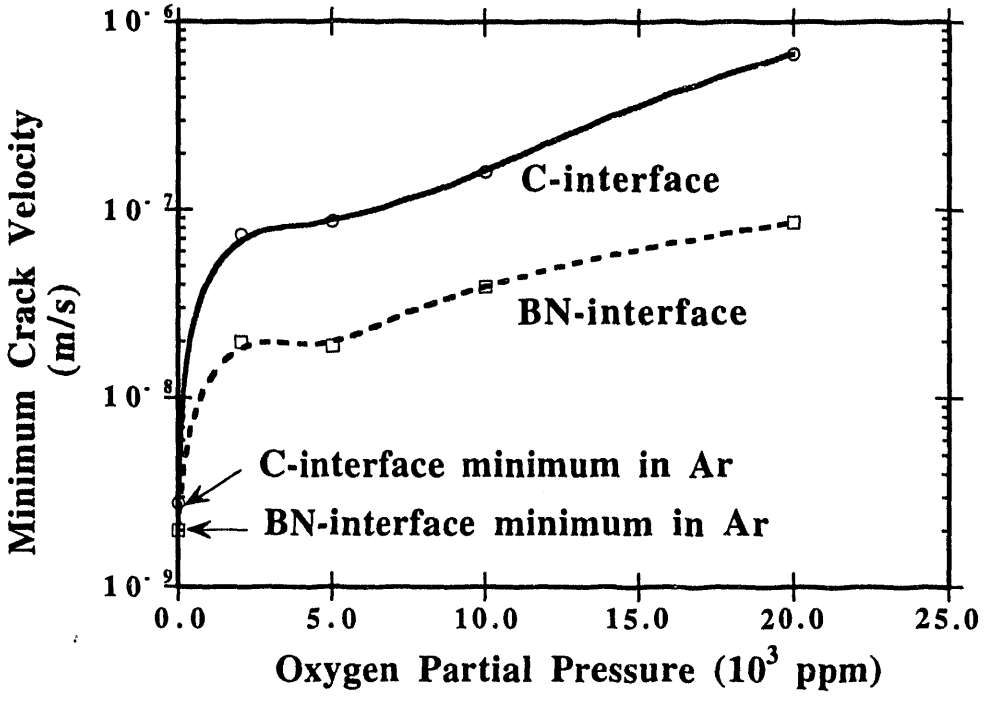

Figure 7. Minimum or limiting crack velocity in C and BN-interface materials as a function of oxygen partial pressure at 1100°C.

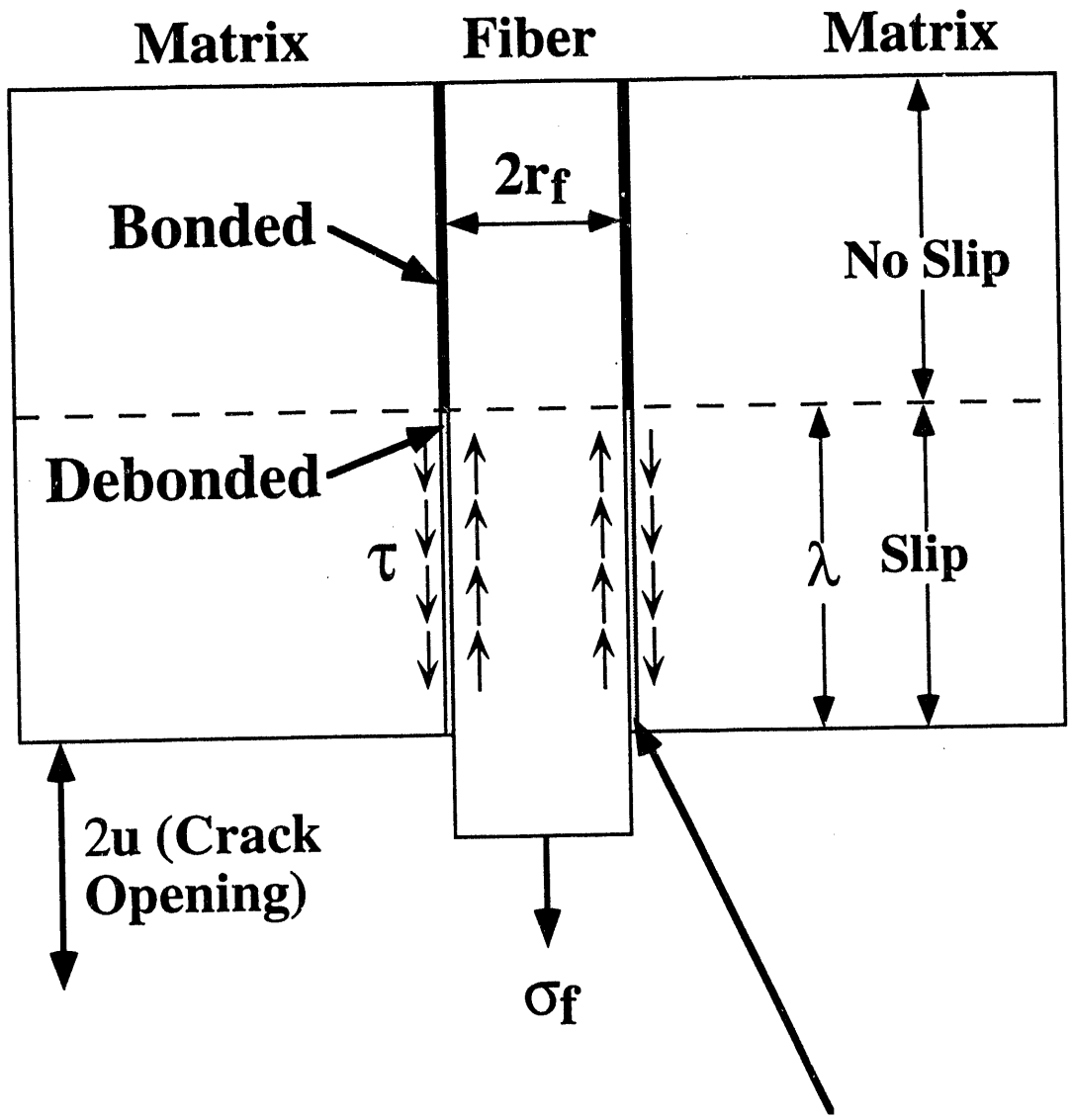

Oxygen ingress occurs along Fiber/Matrix interface and increases λ. Thus, λ and τ become time-dependent in this model.

Figure 8. Schematic diagram of fiber debond model showing λ, τ, u, and σ_f.

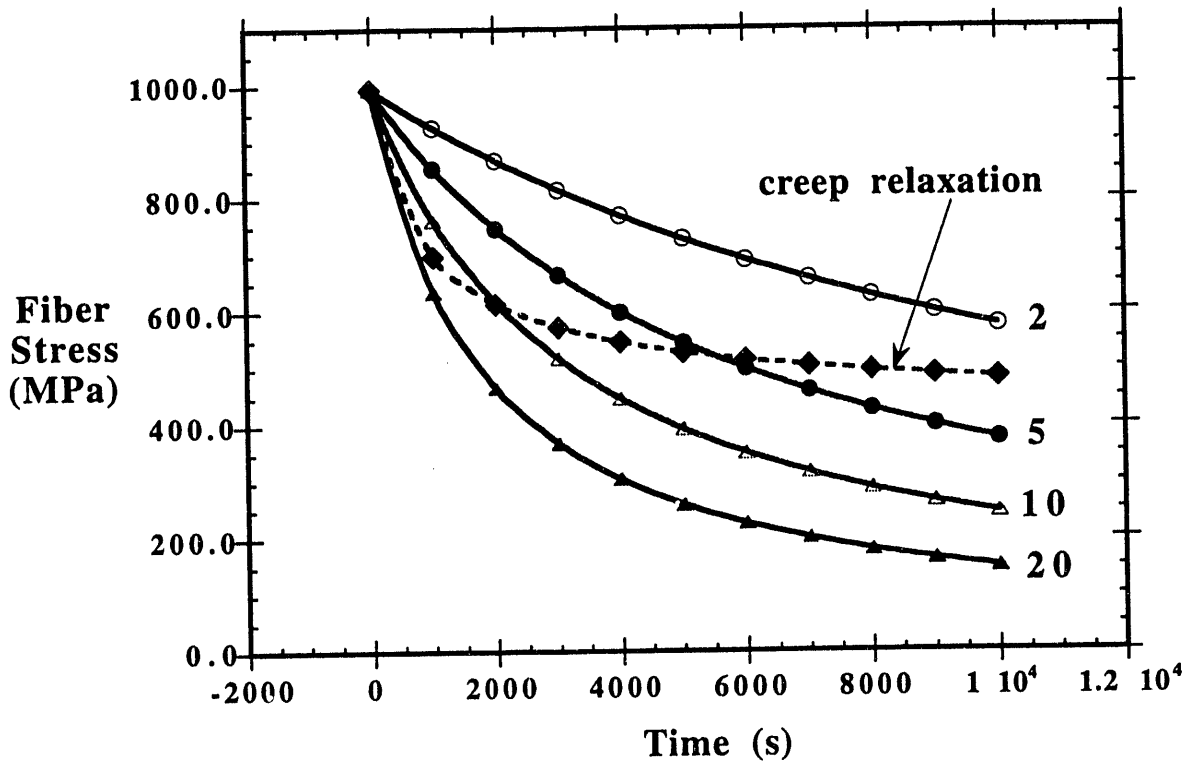

Figure 9. Stress in a bridging fiber as a function of time for pure Ar (fiber creep only) and in varying pO2 levels. The fiber is initially at a stress of 1 GPa and relaxes according to the model described in the text.

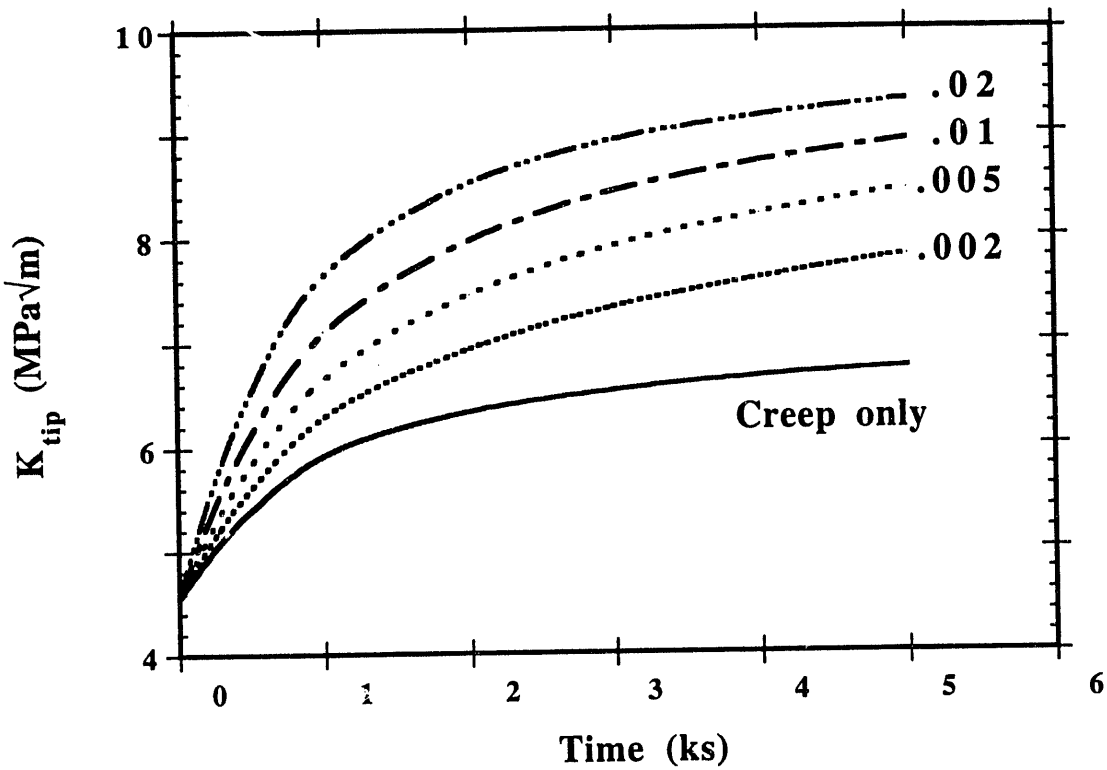

Figure 10. Ktip as a function of time using the 2D model to account for fiber creep and interface removal relaxation events. Addition of oxygen can be seen to increase the relaxation rate compared to fiber creep only.

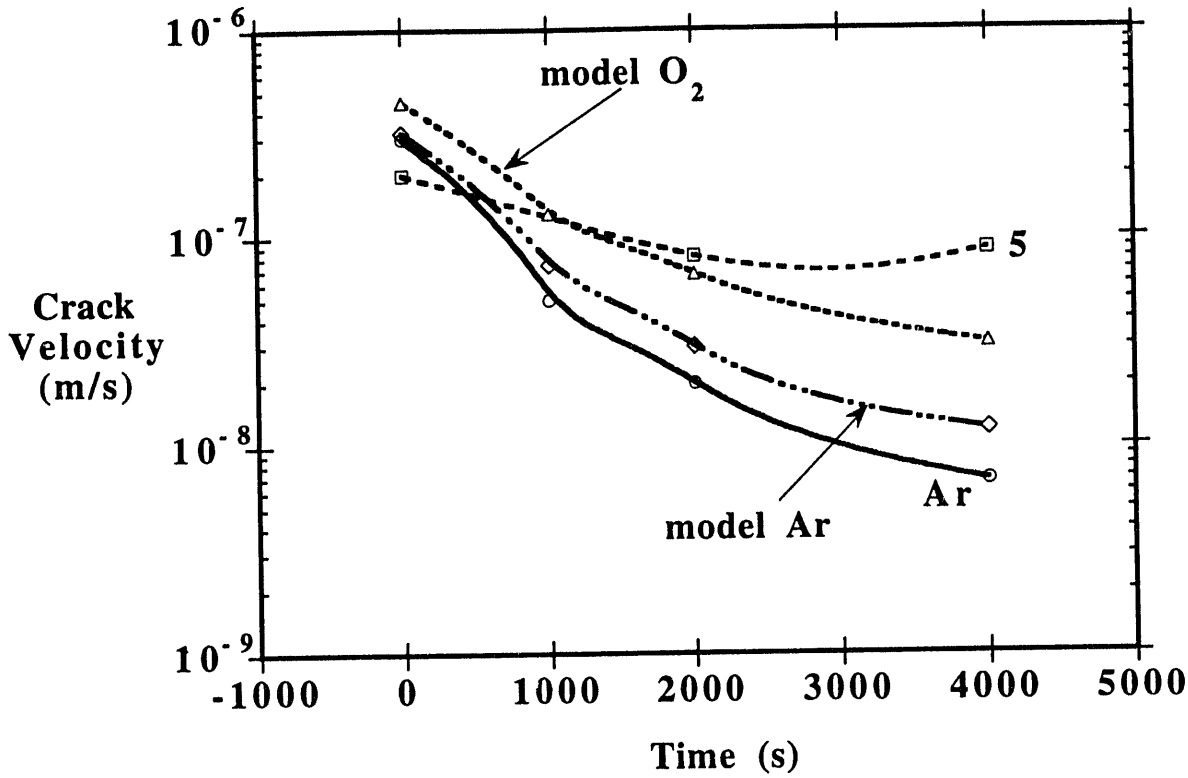

Figure 11. Calculated crack velocities for pure Ar (fiber creep only) and pO2 equal to 0.005 (5000 ppm) showing the increase in velocity associated with interface removal in addition to fiber creep relaxation.

DATE
FILMED
11/1/94

END